Supporting Information

Heavy Mediator at Quantum Dot/Graphene Heterojunction for Efficient Charge Carrier Transfer: Alternative Approach for High Performance Optoelectronic Devices

Rapti Ghosh,[1,3,4,7] Kanchan Yadav,[1,5,8] Monika Kataria,[1,3,4,7] Hung-I Lin,[6,7] Christy Roshini Paul Inbaraj,[5,7,10] Yu-Ming Liao,[5,7] Yen Nguyen,[6,7] Cheng-Hsin Lu,[11] Mario Hofmann,[7] Raman Sankar,[2,9] Wei-Heng Shih,[11] Ya-Ping Hsieh,[1,4] and Yang-Fang Chen[7,12]*

[1]Institute of Atomic and Molecular Sciences, Academia Sinica, Taipei 115, Taiwan

[2]Institute of Physics, Academia Sinica, Taipei 11529, Taiwan

[3]Department of Physics, National Central University, Chung-Li 320, Taiwan

[4]Molecular Science and Technology Program, Taiwan International Graduate Program, Institute of Atomic and Molecular Sciences, Academia Sinica, Taipei 115, Taiwan

[5]Nano Science and Technology Program, Taiwan International Graduate Program, Institute of Physics, Academia Sinica, Taipei 106, Taiwan

[6]Graduate Institute of Applied Physics, National Taiwan University, Taipei 106, Taiwan

[7]Department of Physics, National Taiwan University, Taipei 106, Taiwan

[8]Department of Chemistry, National Taiwan University, Taipei 106, Taiwan

[9]Center for Condensed Matter Sciences, National Taiwan University, Taipei 10617, Taiwan

[10]Department of Engineering and System Sciences, National Tsing Hua University, Hsinchu 30013, Taiwan

[11]Department of Material Sciences and Engineering, Drexel University, Philadelphia, PA 19104, USA

[12]Advanced Research Centre for Green Materials Science and Technology, National Taiwan University, Taipei, Taiwan

*corresponding author: Yang-Fang Chen: yfchen@phys.ntu.edu.tw

Ya-Ping Hsieh: yphsieh@gate.sinica.edu.tw

S1. Schematic diagram of device fabrication:

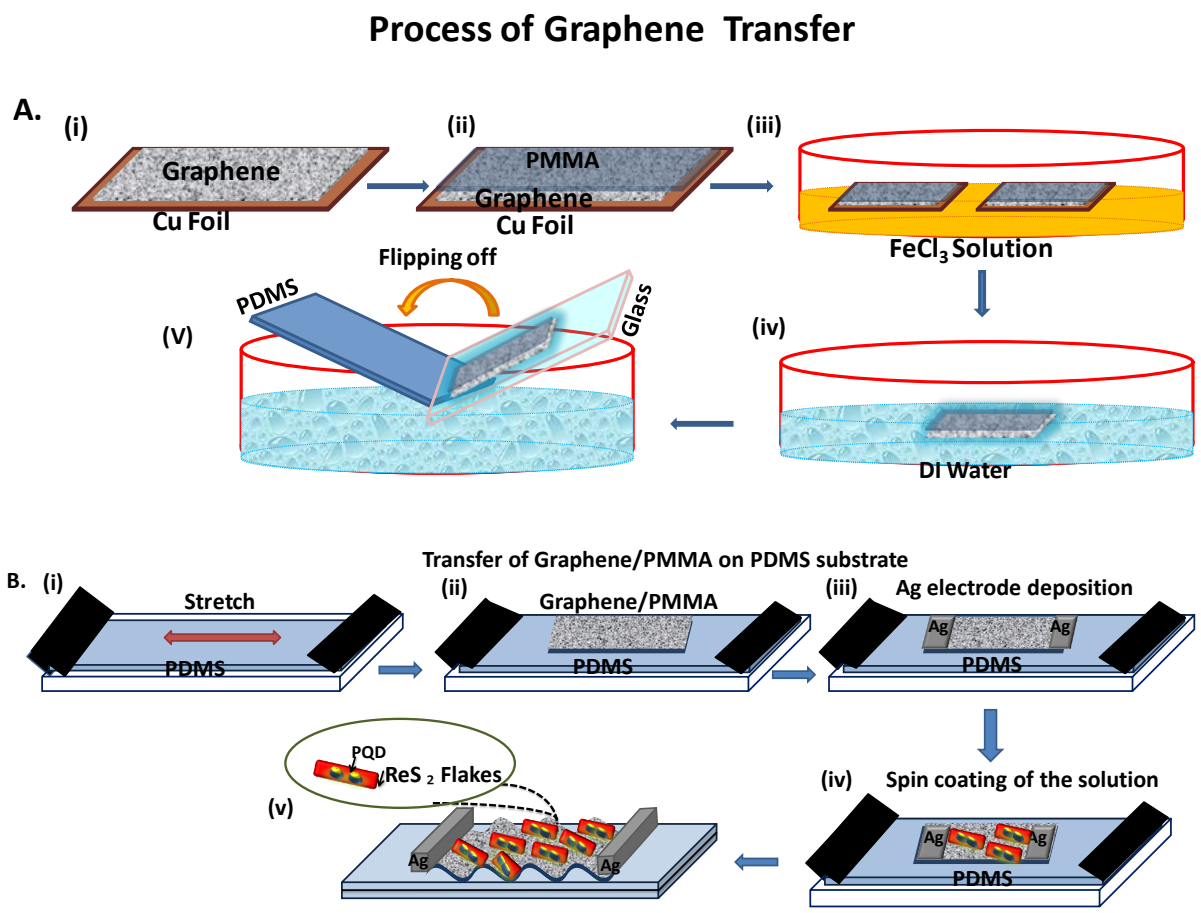

Figure S1. Schematic diagram of device fabrication in different steps:

A. Transfer of graphene: (i) Monolayer graphene growth on Cu foil. (ii) A layer of PMMA is spin coated on graphene. (iii) Cu foil with graphene is cut into small pieces and kept into $FeCl_3$ filled petridish for Cu etching. (iv) Etched graphene is placed in DI water. (v) Graphene is transferred onto the PDMS substrate with the help of a glass slide.

B. (i) PDMS is stretched on the glass substrate and clamped with clip. (ii) Monolayer graphene coated with PMMA is transferred on PDMS substrate. (iii) Ag electrode is grown by shadow masking technique on graphene/PMMA. (iv) ReS_2 bonded with PQD solution is coated on top of the graphene. (v) After releasing the clip, wavy pattern structure is produced.

S2. Optimization of the thickness of the ReS_2-PQD bonded solution:

The appropriate thickness of the active material i.e ReS_2-PQD bonded solution on graphene is obtained through a long optimization process. A particular thickness of the solution is only capable of providing maximum photocurrent along with fast response time. If the concentration of the solution is too thick, then it hinders the flow of charge carriers towards graphene channel. On the other hand, if the solution is too diluted, then only a few ReS_2-PQD bonded flakes will remain in the solution which will not be enough to absorb the right amount of photons and result in a pronounced photocurrent with fast response time. In between, there exists an optimized thickness which is suitable for having a good photodetector.[1]

In order to have the proper thickness, 1 part of the ReS_2-PQD bonded solution is diluted in the 1000 part of solvent 99% pure Ethanol. This diluted solution is then spin coated on the top of graphene in different rotation per minute (RPM) variation such as: i) 5 seconds at 1000 RPM and 25 seconds at 2000 RPM, ii) 5 seconds at 1000 RPM and 25 seconds at 2500 RPM, iii) 5 seconds at 1000 RPM and 25 seconds at 3000 RPM, iv) 5 seconds at 1000 rpm and 25 seconds at 3500 rpm, v) 5 seconds at 1000 rpm and 25 sec at 4000 rpm.

After spin coating, the photocurrent is measured under 325 nm laser illumination of power 80 nW at a bias voltage of 0.1 V. The variation of response time with RPM variation is shown in Figure S3. The optimized response time of the order of 200 ms is obtained for the solution having 1 part of the original ReS_2-PQD bonded solution and 1000 part of Ethanol, spin coated at a speed of 1000 rpm for 5 seconds and 3500 rpm for 25 seconds.

i)

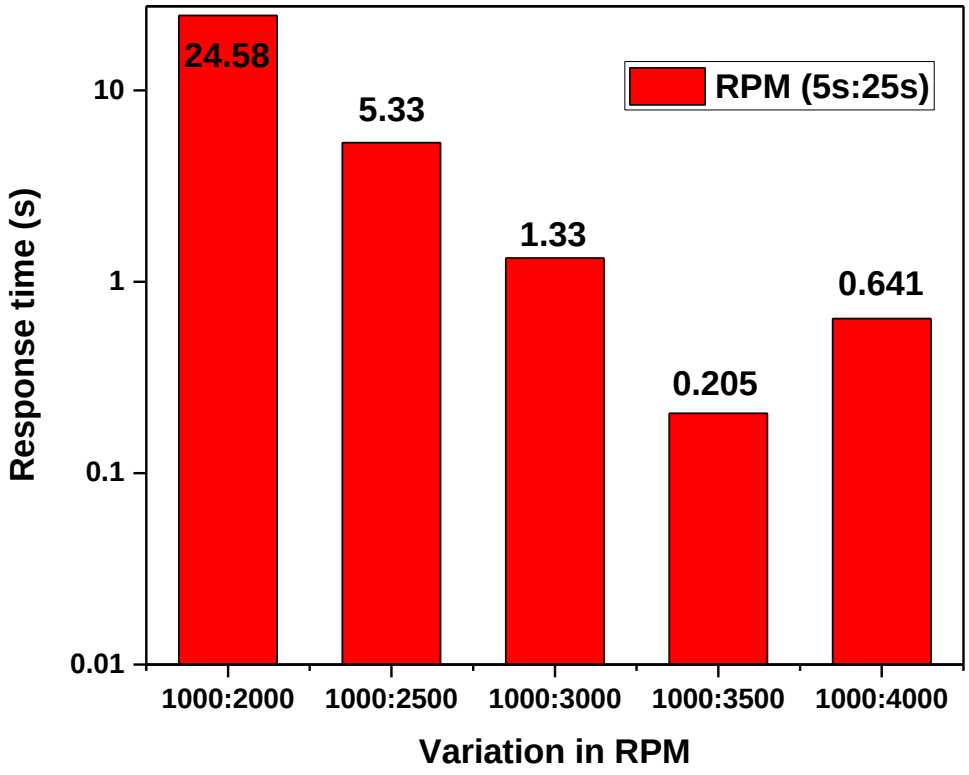
24.58
5.33
1.33
0.205
0.641
RPM (5s:25s)
Response time (s)
10
1
0.1
0.01
1000:2000
1000:2500
1000:3000
1000:3500
1000:4000
Variation in RPM

ii)

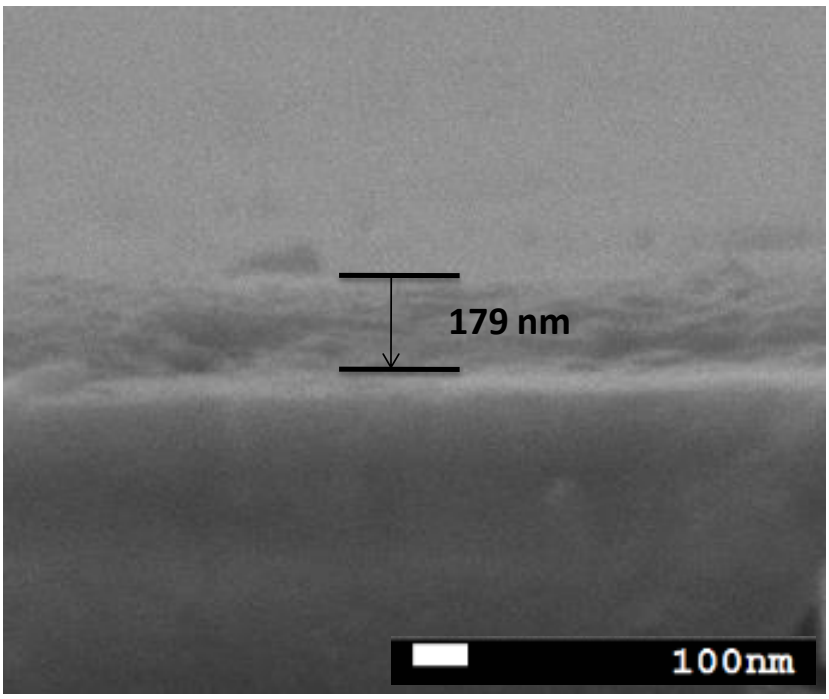
179 nm
100nm

iii)

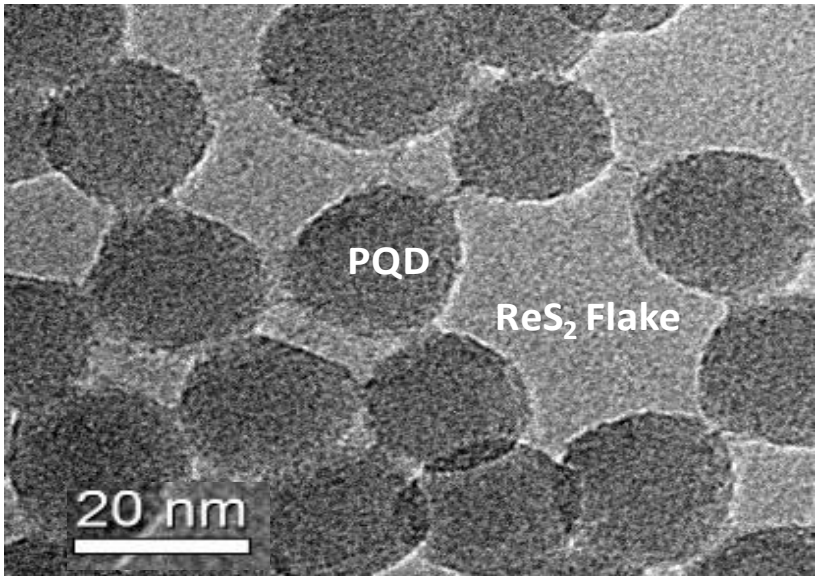

iv)

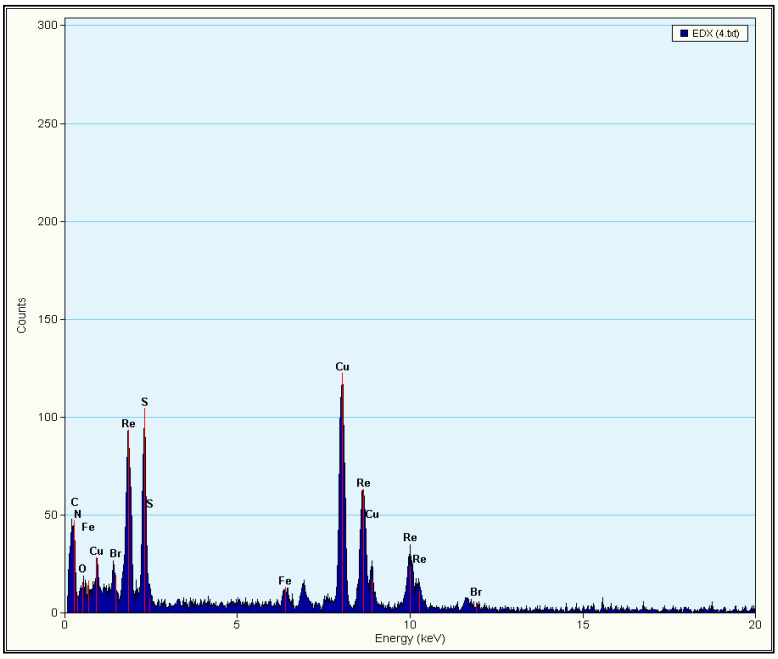

Figure S2. Device optimization by variation of thickness of ReS_2 bonded PQD solution: (i) Histogram showing the variation of photocurrent response time with concentration. (ii) SEM image showing the optimized thickness of the solution after spin coating on the hybrid device. (iii) HRTEM image showing the distribution of PQD on ReS_2 flake. (iv) EDAX image showing the elemental distribution of the components.

S3. Characterization of ReS_2 flake :

The ReS_2 flake is characterized by HRTEM (Figure S3 i) representing a few layers ReS_2 flake having a size approximately 60 nm in length and 40 nm in breadth. The fast Fourier transform (FFT) pattern (inset) of ReS_2 flake confirms the regular crystallographic arrangement of atoms.[2]

The Raman spectrum of ReS_2 flake (Figure S3 ii) has 10 vibrational modes within the range 100-400 cm^{-1} whereas the most prominent peaks are at 150 cm^{-1} and 210.5 cm^{-1} corresponding to in-plane (E_g like) and out of plane (A_g like) vibrational modes, which matches well with the previously reported values.[3]

PL spectrum of few layers ReS_2 flake (Figure S3 iii) represents an emission peak at around 1.45 eV.

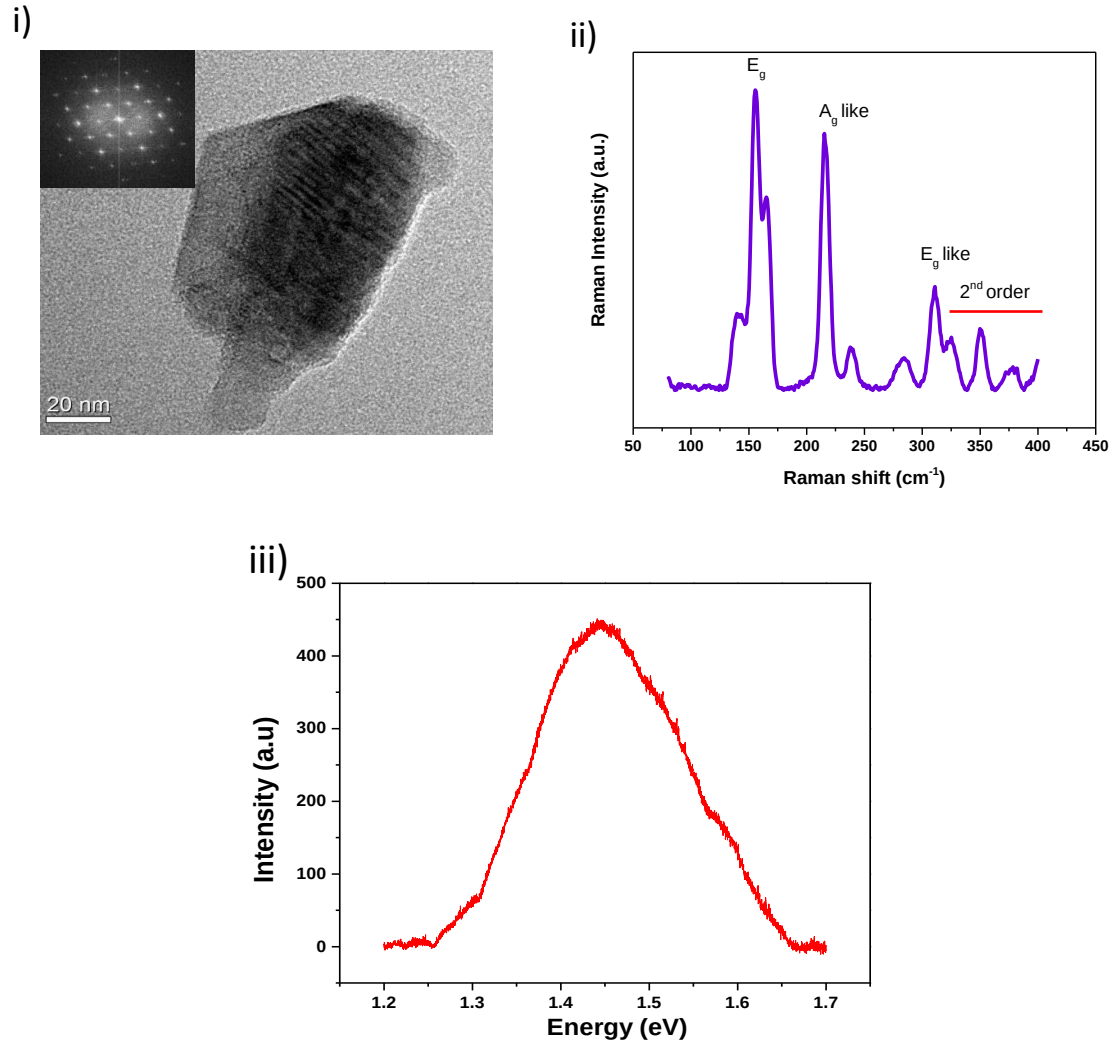

Figure S3. Characterization of few layers ReS_2 flake: (i) Transmission electron microscope (TEM) image of few layer flakes. The inset FFT pattern shows the crystallinity of ReS_2. (ii) Raman spectrum of few layers ReS_2 flake. (iii) Photoluminescence (PL) spectrum of few layer ReS_2 flakes.

S4. Schematic diagram for ReS_2-PQD bonded flake synthesis:

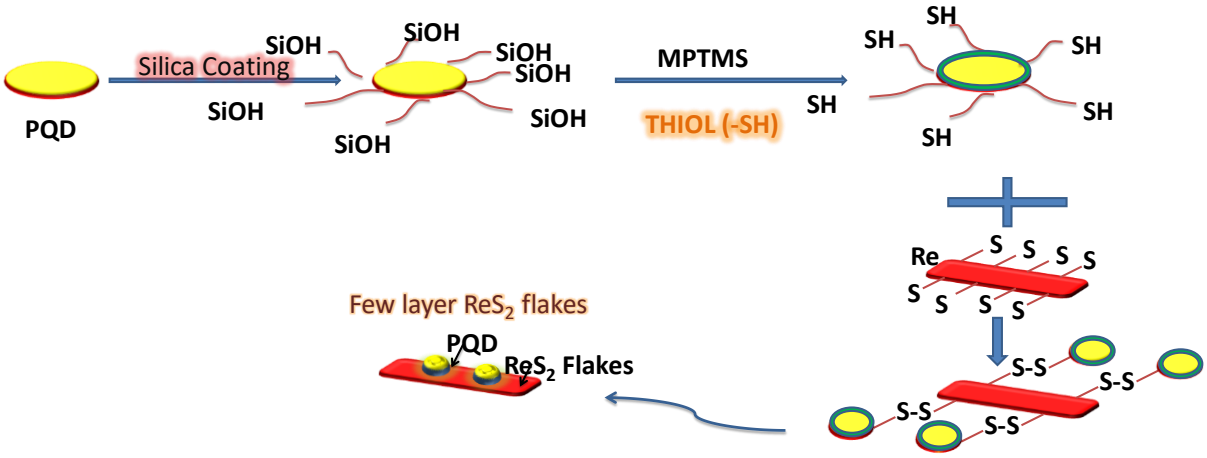

Figure S4. Schematic diagram illustrating the steps of binding of PQD with ReS_2 flake through disulfide bonding.

The Methylammonium Lead Halide perovskite quantum dots were pre-treated before using in the photodetector to avoid degradation issues. In the first stage, the PQDs were coated with a thin layer of silica to provide better environmental stability. Generally treating QDs with an insulating layer enhances its stability but causes a major effect on carrier transport. To circumvent this issue, the coating material should be chosen wisely. According to coordination chemistry, among X, L and Z type ligands X type ligand is more preferable since both the ligand and the nanoparticle contribute one electron to make a strong chemical bond.[4] Because Thiol molecules are X-type ligand, the PQDs were attached with Thiol ligand after silica coating in the next step. Thiol exchanges electron with the Pb molecule of PQD forming stable Pb-S bond, which decreases surface energy and increases conductivity. Even because of the Thiol ligand (X-type), the PQDs show stability in polar solvent Ethanol also. Thus Thiol ligand provides excellent stability without affecting the electronic property of the PQD since the length of the ligand is not long enough to prevent the electron transport.

S5. Zeta Potential Measurement of ReS_2 Bonded with PQD:

Zeta potential tells the surface charge of samples. Since PQDs have Br in the composition, surface charge shows a negative value of - 9 mV. In the next step, after MPTMS modification, zeta potential shifted to - 18.2 mV because MPTMS contains thiol functional group which is negatively charged and further after the formation of PQD-ReS_2, the zeta value shifted to a more negative value (- 23 mV).

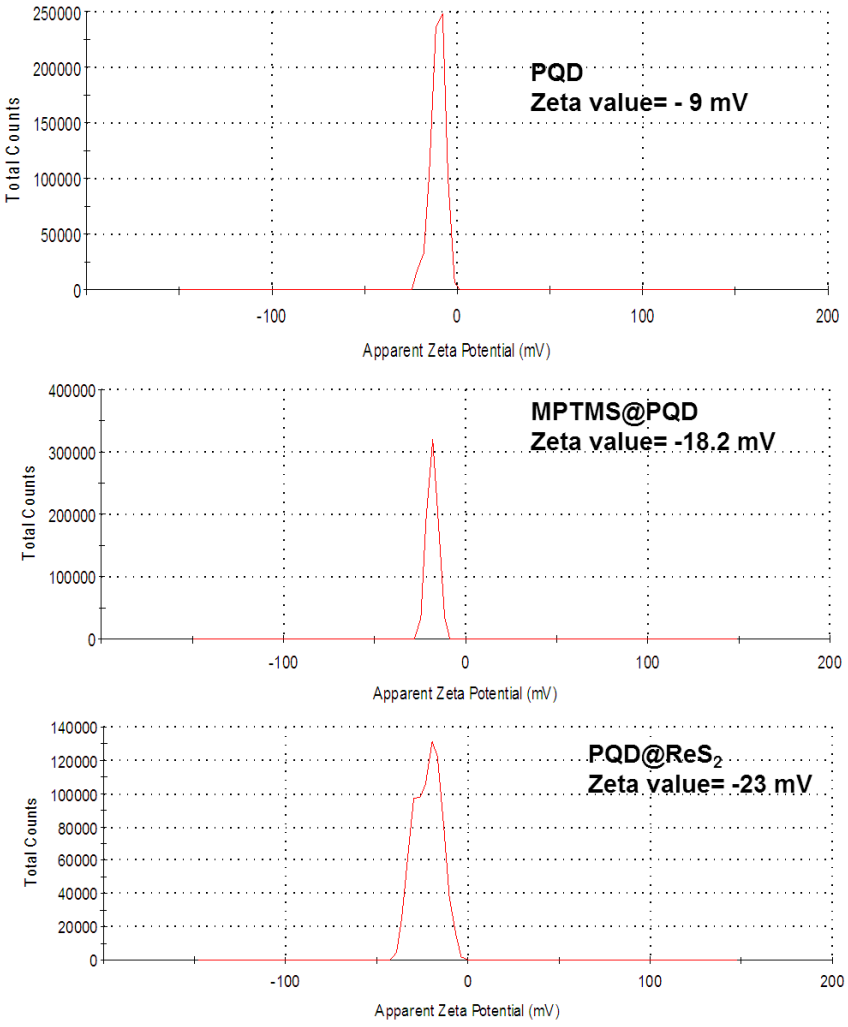

Figure S5. Zeta potential measurement of ReS_2 bonded with PQD.

S6. Characterization of perovskite quantum dot (PQD):

The HRTEM image of PQD (Figure S6 (i)) and the corresponding FFT pattern (inset) of a single nanoparticle clearly reveals the regular crystallographic arrangement of atoms. From the FFT pattern, the crystalline nature of the nanoparticle is revealed.[5]

The photoluminescence (PL) spectrum of PQD (Figure S6 (ii)) represents a narrow PL peak at around 530 nm.

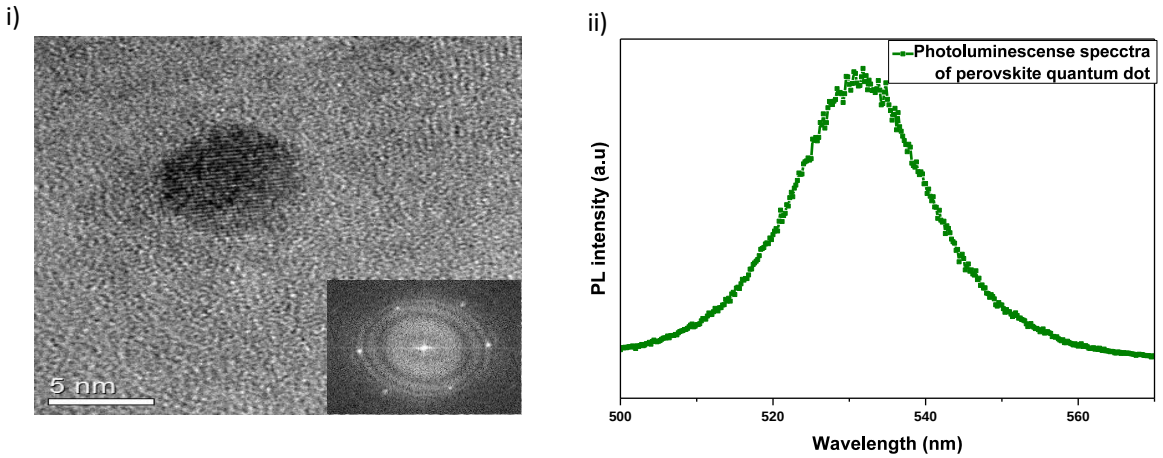

Figure S6. Characterization of perovskite quantum dot: (i) Transmission electron microscope (TEM) image of perovskite quantum dot (PQD). The inset figure is the FFT pattern of it showing polycrystalline behavior. (ii) Photoluminescence (PL) spectrum of PQD.

S7. Calculation of Responsivity, Detectivity and Photocurrent gain:

Measurement of Responsivity:

The formula for measuring the photoresponsivity is given by:

$$\mathbf{R_P = |\Delta I|/P}$$

$|\Delta I|$: Change in photocurrent ($I_{Ph} = I_{ON} - I_{OFF}$)

P: Power used by the device ((Power of the laser source/spot size) × channel length)

Detectivity:

$$\mathbf{D = R_P S^{1/2} / (2e\ I_D)^{1/2}}$$

R_P :Photoresponsivity

S: Effective area

E: Electronic charge

I_D : Dark current of the device

Photocurrent gain:

$$\mathbf{\eta = R_P\ h\ c/e\lambda}$$

R_P : Photoresponsivity

h : Planck's constant

c: Velocity of light

e: Electronic charge

λ: Wavelength of light

for an example, if a photo current of 93.6 μA is measured under a laser (325 nm) of 530 nW power of spot size 0.06 cm^2 on the device having channel length 205 μm×45 μm then corresponding values will be:-

$R_P = | \Delta I|/P$

$= (93.6\ \mu A)/((530\ nW/0.06\ cm^2) \times 205\ \mu m \times 45\ \mu m)$

$= 1.2 \times 10^5\ A/W$

$D= R_P\ S^{1/2} / (2e\ I_D)^{1/2}$

$= (1.2 \times 10^5\ A/W) \times (205\ \mu m \times 45\ \mu m)^{1/2}/(2e \times 1.7 \times 10^{-4} A)^{1/2}$; $[I_D= 1.7 \times 10^{-4} A]$

$=1.56 \times 10^{12}$ Jones

$\eta= R_P\ h\ c/e\lambda$

$= ((1.2 \times 10^5\ A/W)/325nm) \times (hc/e)$

$= 4.59 \times 10^5$

S8. Photoluminescence spectra of ReS_2 bonded PQD and ReS_2 bonded PQD/graphene flake:

The photoluminescence spectra have been studied for both ReS_2 bonded PQD with graphene flakes and without graphene flakes. Under the illumination of the 374 nm laser, the decrement of PL intensity of ReS_2 bonded PQD has been observed in the presence of graphene flakes because of charge transferring mechanism which results in quenching of PL intensity.

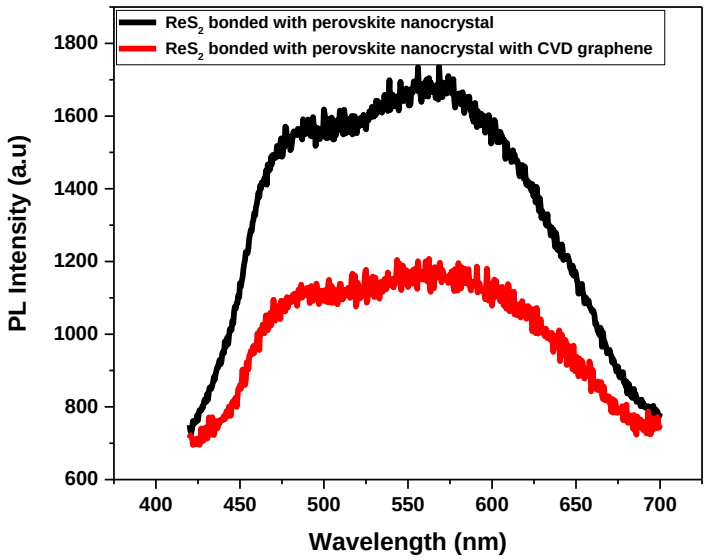

Figure S8. Photoluminescence spectra of ReS_2 bonded PQD and ReS_2 bonded PQD/graphene flake.

S9. Wavelength dependent photoresponsivity of the device:

The device has the capability of withstanding wavelength dependence responsivity. Graphene can absorb the light across the whole spectral regime whereas ReS_2 at NIR and PQD at the visible range. Because of the variation of spectral absorptivity at different wavelengths, we witnessed a spectral dependent responsivity as shown below.

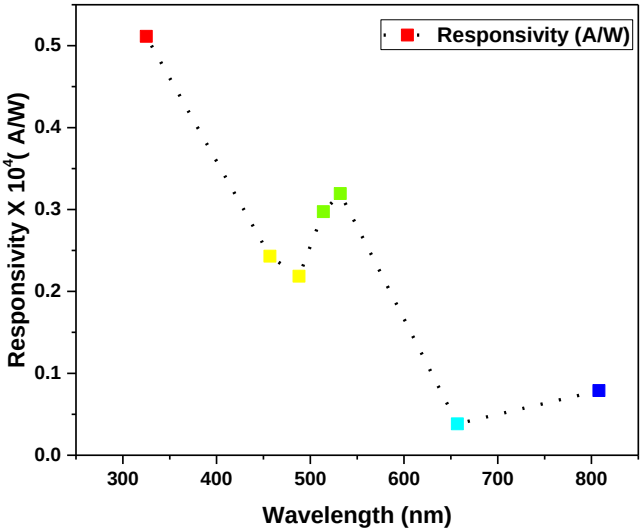

Figure S9. Photoresponsivity of the device at different wavelengths

S10. Photoconfinement mechanism in wavy pattern device:

The decrement of photocurrent with the increase of strain occurs due to the phenomena of photon confinement effect which varies with the change of the size of the wave. When the device is under 0% strain (Released state), the height of the waves is maximum resulting in maximum trapping of photons which thereby internally reflected for multiple times producing maximum photocurrent and hence increases the radiation density. On the other hand, with the increase of strain since the height of the wave is decreased, the wavy structure becomes more flattened and fewer photons trapping occurs causing a decrement of the radiation intensity per unit area of the wave.[6] Thus the longitudinal strain has a major impact on the photocurrent of the device which is further analyzed in S8.

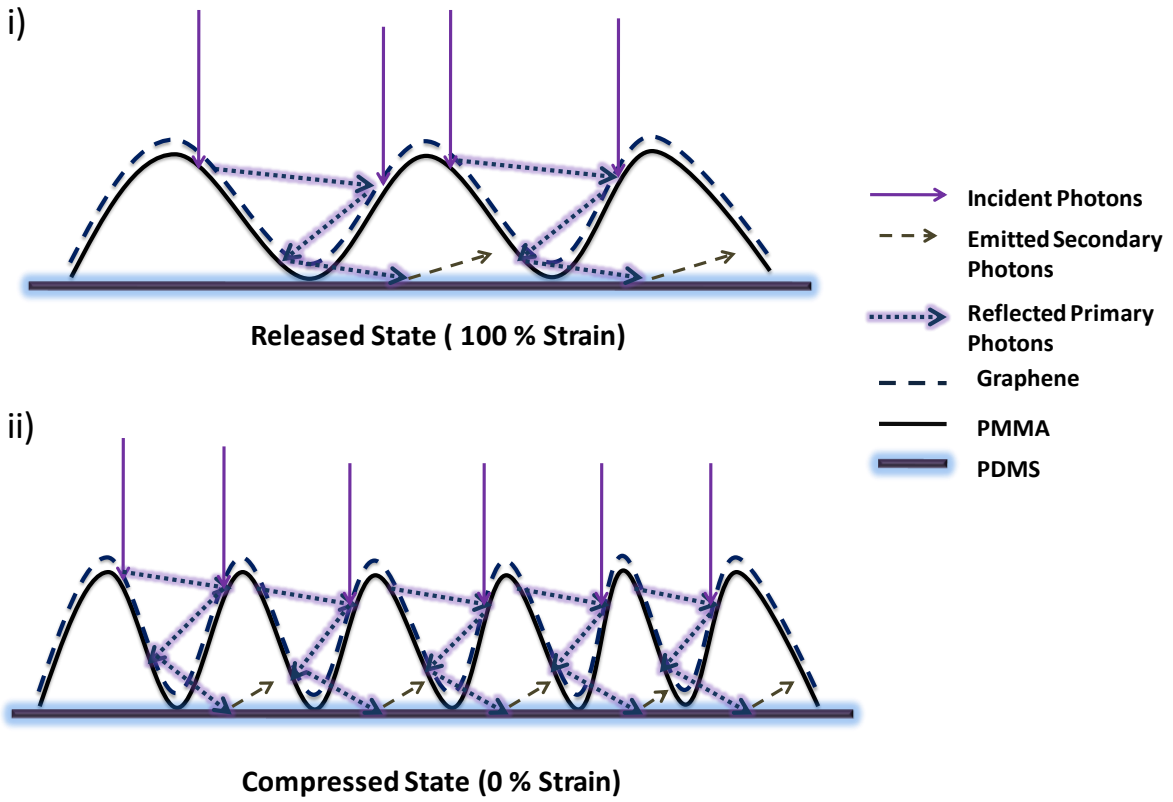

Figure S10. Photoconfinement effect in (i) stretched and (ii) released state of the wavy pattern device.

S11. Quantitative analysis of electron scattering mechanism in wavy structured graphene:

The incident photons get captured in the walls of wavy structured graphene giving birth to the phenomena of photon confinement effect. Let **v** is the height of the wave and **u** is the radius of a single wave. Now $\mathbf{v_0}$ is the height of the wave in the released state or 0% strain state. Therefore the strain can be defined as:-

$$\varepsilon = \Delta v / v_0;\ \varepsilon = (v - v_0) / v_0$$

Therefore, $v = v_0 (1 + \varepsilon)$

Again, if **w** is the length from the bottom to the top of the wave then,

$$w^2 = u^2 + v^2$$

Here if the radius of the wave = **r** is a quadratic function of strain then the change in conductivity ratio can be written as:-

$$\delta p = c \times (v^4 / \varepsilon)$$

c = constant related to Planks constant **h**

Since the height of the wave in both stretched state and released state are in a nanometer scale, the higher powers can be neglected. Simplifying the equation:

$$\delta p = (c / \varepsilon) (w^2 - u_0^2)$$

u_0 = radius of the wave in the released state or 0% strain state

Therefore, it can be concluded that conductivity is inversely proportional to strain.

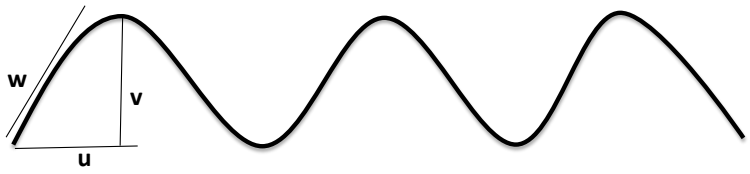

Stretched State (100 % Strain)

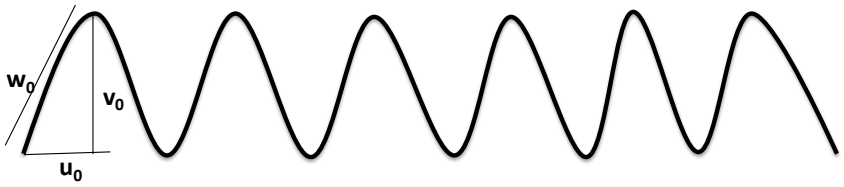

Released State (0 % Strain)

S12. Transmission spectra of planar and wavy pattern PDMS structure:

The transmission spectrum of planar graphene/PDMS substrate shows a better optical transmittency compared to its wavy patterned counterpart. It can be concluded that because of the presence of wavy structure in graphene/PDMS, photon confinement occurs which results in enhancing the absorption of incident photons.[7]

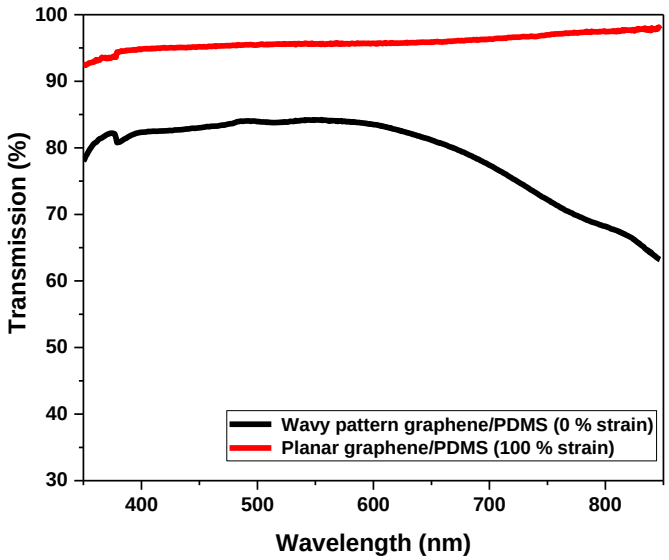

Figure S12. Optical transmission spectra of planar and wavy pattern graphene on PDMS.

S13. Raman spectra of graphene over wavy patterned PDMS:

The Raman spectrum of bare PDMS is observed at 1260 cm^{-1} and 1420 cm^{-1} due to the presence of vibrational peaks of Si-O-Si group and CH_3 groups, respectively[8].

The Raman signal of graphene exhibits distinguishable G and 2D peaks whereas D peak of Raman spectrum of graphene is less significant. This concludes the almost defect free characteristic of graphene layer. The ratio of G and 2D peak confirms the monolayer thickness of graphene.

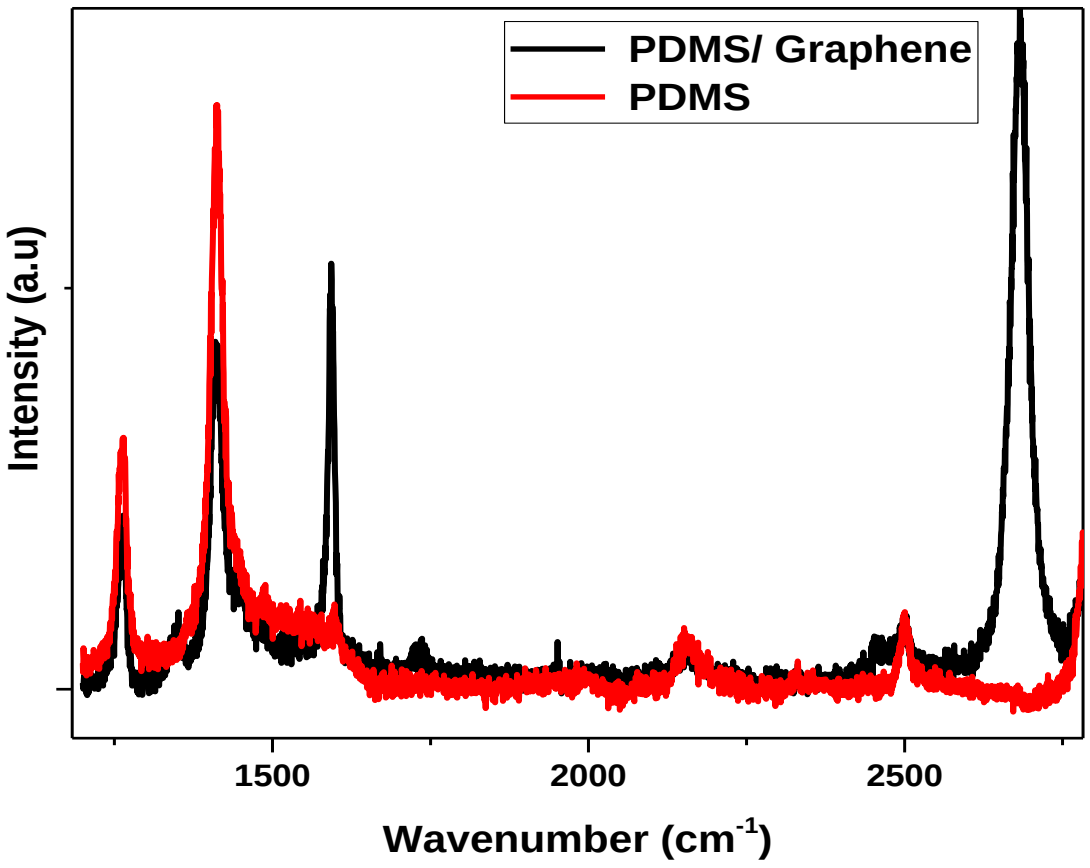

Figure S13. Raman spectra of PDMS and graphene on PDMS.

S14. Stretchability and wearability of the device:

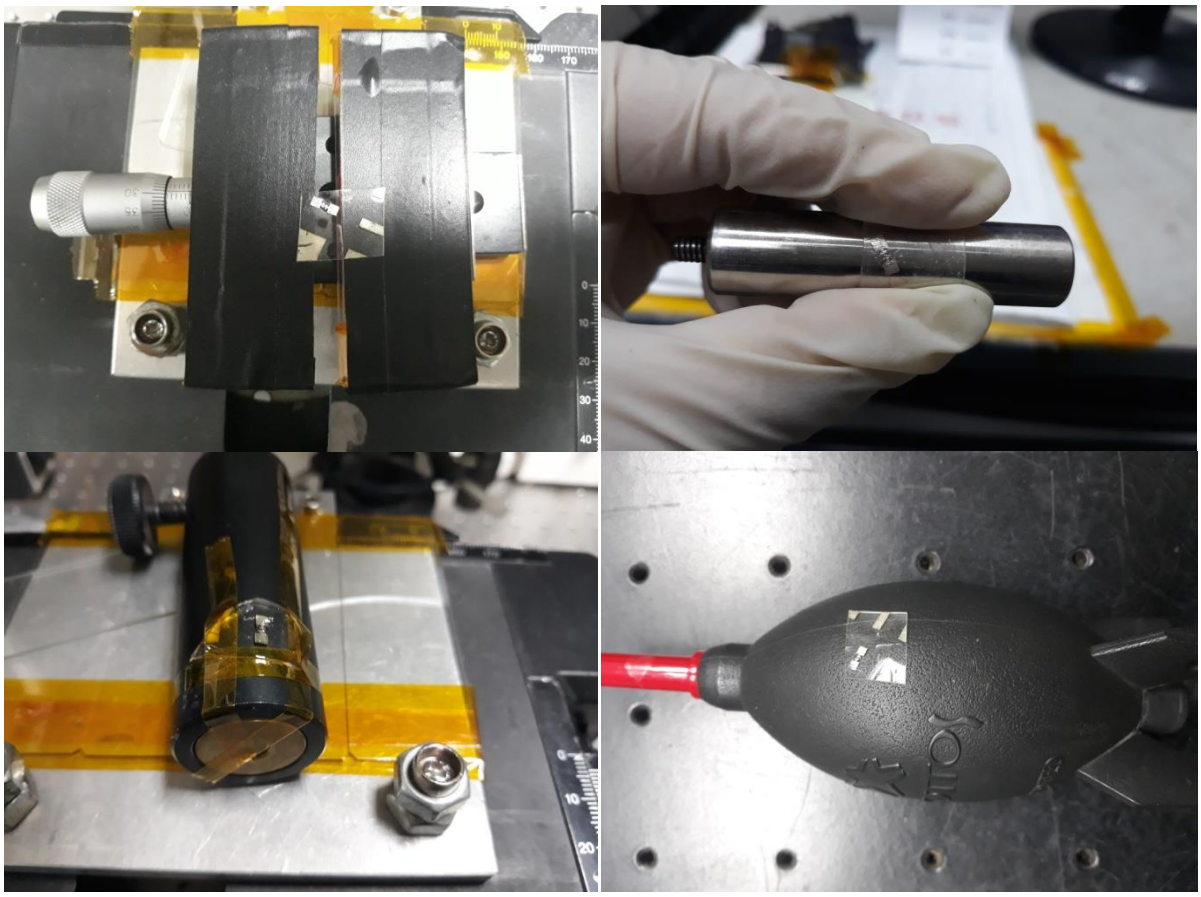

Figure S14. The experimental set up used to study the longitudinal strain and bending strain keeping it on different cylindrical apparatus with various curvatures. The wearability as well as transparency is proven by keeping the device on different solid substances.

S15. Stability of the device performance: measurement of the photocurrent at different period of time:

The chemical stability of the device was judged for a period of 90 days where it did not result in much alteration of photocurrent. The stability of the perovskite layer and the ReS_2 layer along with the CVD grown graphene provides the durability to the device.

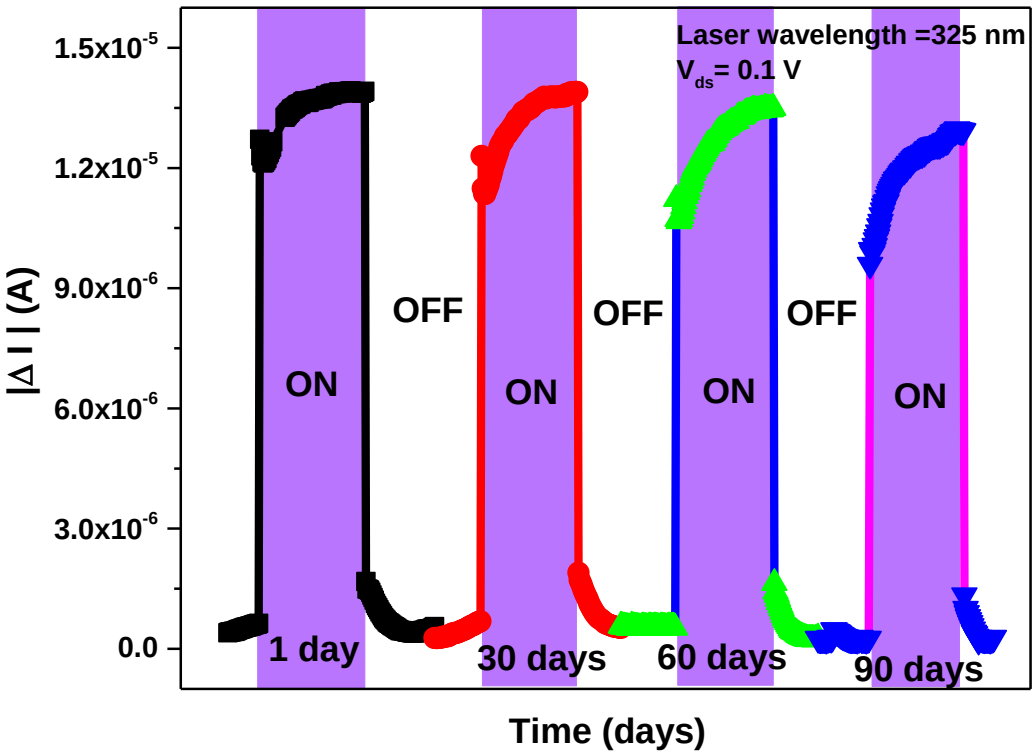

Figure S15. Temporal photoresponse at different periods of time measuring the stability.

Table S1. Comparative study among different stretchable photodetectors:-

GQD: Graphene Quantum Dot; UCNP: Up Conversion Nanoparticle; MOF: Metal Organic Frame Work; VHB: Very High Bonded Film; PQD: Perovskite Quantum Dot; rGO: Reduced Graphene Oxide; SWNT: Single Walled (carbon) Nanotube.

Category	Device architect	Responsivity ($A\ W^{-1}$)	Response time
Stretchability	PDMS/graphene/GQD/Galinstan electrode[1]	700 at 1V	
	PDMS/graphene/UCNP/Ag electrode[7]	190 at 1V	< 0.2 s
	PDMS/graphene/MOF/Au electrode[6]	10^6 at 1V	< 0.2 s
	Pyramidal PDMS/graphene/UCNP/Ag electrode[8]	800 at 1V	
	VHB/graphene/perovskite microwire/Au electrode[9]	0.022 at 0.01 V	0.068 s
	Graphene/PEDOT/TiO_2/PbS QD/MoO_3/Au[10]	0.13 at 0V	
	PET/Porphyrin/SWNT/graphene electrode[11]	3.1×10^{-3} at -1V	> 100 s
	Ni/ZnO/Ag/graphene/Ag[12]	0.27 at 1V	6 s
	Mica/rGO-ZnO/Ag electrode[13]	3.24 at 1V	17.9 s
This work	PDMS/graphene/ReS_2/PQD/Ag electrode	10^7 at 1V	< 0.2 s

REFERENCES:

1. Haider, G.; Roy, P.; Chiang, C.-W.; Tan, W.-C.; Liou, Y.-R.; Chang, H.-T.; Liang, C.-T.; Shih, W.-H.; Chen, Y.-F., Electrical-Polarization-Induced Ultrahigh Responsivity Photodetectors Based on Graphene and Graphene Quantum Dots. *Adv. Funct. Mater.* **2016,** *26*, 620-628.

2. Hafeez, M.; Gan, L.; Li, H.; Ma, Y.; Zhai, T., Large-Area Bilayer ReS_2 Film/Multilayer ReS_2 Flakes Synthesized by Chemical Vapor Deposition for High Performance Photodetectors. **2016**; Vol. 26.

3. Tongay, S.; Sahin, H.; Ko, C.; Luce, A.; Fan, W.; Liu, K.; Zhou, J.; Huang, Y.-S.; Ho, C.-H.; Yan, J.; Ogletree, D. F.; Aloni, S.; Ji, J.; Li, S.; Li, J.; Peeters, F. M.; Wu, J., Monolayer Behaviour in Bulk ReS_2 Due to Electronic and Vibrational Decoupling. *Nat. Commun.* **2014,** *5*, 3252.

4. Ruan, L.; Shen, W.; Wang, A.; Zhou, Q.; Zhang, H.; Deng, Z., Stable and Conductive Lead Halide Perovskites Facilitated by X-type Ligands. *Nanoscale* **2017,** *9*, 7252-7259.

5. Schmidt, L. C.; Pertegás, A.; González-Carrero, S.; Malinkiewicz, O.; Agouram, S.; Mínguez Espallargas, G.; Bolink, H. J.; Galian, R. E.; Pérez-Prieto, J., Nontemplate Synthesis of $CH_3NH_3PbBr_3$ Perovskite Nanoparticles. *J. Am. Chem. Soc.* **2014,** *136*, 850-853.

6. Bera, K. P.; Haider, G.; Usman, M.; Roy, P. K.; Lin, H.-I.; Liao, Y.-M.; Inbaraj, C. R. P.; Liou, Y.-R.; Kataria, M.; Lu, K.-L.; Chen, Y.-F., Trapped Photons Induced Ultrahigh External Quantum Efficiency and Photoresponsivity in Hybrid Graphene/Metal-Organic Framework Broadband Wearable Photodetectors. *Adv. Funct. Mater.* **2018,** *28*, 1804802.

7. Kataria, M.; Yadav, K.; Haider, G.; Liao, Y. M.; Liou, Y.-R.; Cai, S.-Y.; Lin, H.-i.; Chen, Y. H.; Paul Inbaraj, C. R.; Bera, K. P.; Lee, H. M.; Chen, Y.-T.; Wang, W.-H.; Chen, Y. F., Transparent, Wearable, Broadband, and Highly Sensitive Upconversion Nanoparticles and Graphene-Based Hybrid Photodetectors. *ACS Photonics* **2018,** *5*, 2336-2347.

8. Kataria, M.; Yadav, K.; Cai, S.-Y.; Liao, Y.-M.; Lin, H.-I.; Shen, T. L.; Chen, Y.-H.; Chen, Y.-T.; Wang, W.-H.; Chen, Y.-F., Highly Sensitive, Visible Blind, Wearable, and Omnidirectional Near-Infrared Photodetectors. *ACS Nano* **2018,** *12*, 9596-9607.

9. Ding, J.; Fang, H.; Lian, Z.; Lv, Q.; Sun, J.-L.; Yan, Q., High-Performance Stretchable Photodetector Based on $CH_3NH_3PbI_3$ Microwires and Graphene. *Nanoscale* **2018,** *10*, 10538-10544.

10. Kim, T.-H.; Lee, C.-S.; Kim, S.; Hur, J.; Lee, S.; Shin, K. W.; Yoon, Y.-Z.; Choi, M. K.; Yang, J.; Kim, D.-H.; Hyeon, T.; Park, S.; Hwang, S., Fully Stretchable Optoelectronic Sensors Based on Colloidal Quantum Dots for Sensing Photoplethysmographic Signals. *ACS Nano* **2017,** *11*, 5992-6003.

11. Pyo, S.; Kim, W.; Jung, H.-I.; Choi, J.; Kim, J., Photodetectors: Heterogeneous Integration of Carbon-Nanotube–Graphene for High-Performance, Flexible, and Transparent Photodetectors. *Small* **2017,** *13*, 1700918.

12. Zhu, Z.; Gu, Y.; Wang, S.; Zou, Y.; Zeng, H., Improving Wearable Photodetector Textiles via Precise Energy Level Alignment and Plasmonic Effect. *Adv. Electron. Mater.* **2017,** *3*, 1700281.

13. An, J.; Le, T. S. D.; Lim, C. H. J.; Tran, V. T.; Zhan, Z.; Gao, Y.; Zheng, L.; Sun, G.; Kim, Y. J., Single-Step Selective Laser Writing of Flexible Photodetectors for Wearable Optoelectronics. *Adv. Sci.* **2018,** *5*, 1800496.